

RESEARCH ARTICLE

Spectral filtering effect on multi-pulsing induced by chirped fiber Bragg grating in dispersion-managed mode-locked Yb-doped fiber lasers

Dongyu Yan, Bowen Liu, Defeng Zou, Jie Guo, Yuxi Chu, Youjian Song, and Minglie Hu

Ultrafast Laser Laboratory, School of Precision Instrument and Optoelectronics Engineering, Key Laboratory of Optoelectronic Information Technology (Ministry of Education), Tianjin University, Tianjin 300072, China

(Received 13 March 2021; revised 13 May 2021; accepted 2 July 2021)

Abstract

We numerically and experimentally investigate the multi-pulsing mechanism in a dispersion-managed mode-locked Yb-doped fiber laser. Multi-pulsing occurs primarily owing to the inherent filtering effect of the chirped fiber Bragg grating. The spectral filtering effect restricts the spectral broadening induced by self-phase modulation and causes extra loss, leading to a decreased pump power threshold for the multi-pulsing state. Numerical simulations show that multi-pulsing emerges at a lower pump power when the spectral filter bandwidth becomes narrower. In the experiment, the spectral width increases as the net cavity dispersion approaches zero. Pulses with wider spectral widths experience more loss from the spectral filtering effect, leading to a decreased pump power threshold for multi-pulsing. Therefore, the net cavity dispersion also has an impact on the multi-pulsing threshold. Based on this conclusion, we devise a strategy to obtain single-pulsing operation with the shortest pulse width and the highest pulse energy.

Keywords: fiber optics oscillators; nonlinear fiber optics; ultrafast lasers

1. Introduction

Low-noise mode-locked lasers enable many applications such as precise frequency comb generation^[1,2] optical communications^[3], timing synchronization^[4], and low-phase-noise microwave signal generation^[5]. Among the various ways to achieve low-noise femtosecond lasers, passively mode-locked fiber lasers are highly attractive, benefiting from compactness, robustness, high efficiency, and good beam quality^[6]. Major pulse-shaping mechanisms include solitons^[7], dispersion-managed (DM) solitons^[8], similaritons^[9], and dissipative solitons^[10]. In particular, DM fiber lasers operating at near-zero net cavity dispersion (NCD) can achieve the lowest timing jitter and intensity noise^[11,12]. In our previous study, stable mode-locking can operate near-zero NCD by using saturable absorbers with a high modulation depth^[13]. Higher pulse energy is favorable to further reduce the timing jitter^[14] and improve the performance of low-noise applications. However, with an increased

pump power, the achievable pulse energy is limited by the intrinsic multi-pulsing phenomenon^[15,16]. One possible origin of multi-pulsing is the overdriving of the saturable absorber^[17,18], which is the case for saturable absorbers with non-monotonic response functions such as nonlinear polarization rotation and nonlinear optical loop mirrors. Another possible cause of multi-pulsing is the excessive amount of nonlinear phase accumulation induced by self-phase modulation (SPM)^[19].

A recent theoretical study has investigated the spectral filtering effect on the multi-pulsing dynamics in DM fiber lasers. With an increased pump power, the spectral width increases to a critical point before the onset of multi-pulsing. This critical spectral width (CSW) varies almost linearly with the spectral filter bandwidth. Thus, dissipative spectral filtering can also play a decisive role in the generation of multiple pulses^[20]. In DM mode-locked Yb-doped fiber (YDF) lasers, chirped fiber Bragg gratings (CFBGs) have been utilized for dispersion compensation^[21,22]. CFBGs are attractive because of their compactness, all-fiber configuration, and low splice loss. To obtain a smooth reflection spectrum, apodization is commonly used to suppress the

Correspondence to: B. Liu, School of Precision Instrument and Optoelectronics Engineering, Tianjin University, Tianjin 300072, China. Email: bwliu@tju.edu.cn

oscillations and sidelobes^[23]. Unfortunately, the reflection bandwidth of the apodized CFBG is much narrower than the gain bandwidth of the YDF, leading to a strong spectral filtering effect. This CFBG-induced spectral filtering effect potentially causes multi-pulsing in DM mode-locked YDF lasers.

In this paper, we experimentally investigate the effect of spectral filtering on multi-pulsing in DM mode-locked fiber lasers. The spectral width of a typical DM fiber laser varies monotonically with the NCD in the normal and anomalous dispersion regimes, respectively^[24,25]. For a fixed spectral filter bandwidth, pulses with wider spectral widths experience more loss, and hence the pump power threshold for multi-pulsing is reduced. Consequently, the NCD has an impact on the multi-pulsing dynamics in DM mode-locked fiber lasers. In the experiment, we demonstrate that the pump power threshold for multi-pulsing decreases as the NCD approaches zero. The maximum single pulse energy can be increased to 0.42 nJ by operating the laser at a relatively large NCD^[13]. We also observe that the CSW at the critical point is approximately constant, regardless of the NCD. The largest full-width at half-maximum (FWHM) spectral width obtained is 20.6 nm, which is limited by the 17-nm CFBG reflection bandwidth. The pulses are dechirped to 108 fs by using a hybrid grating-prism compressor. We also perform numerical simulations to investigate the spectral filtering effect on the multi-pulsing dynamics. The pump power threshold for multi-pulsing state decreases as the NCD approaches zero. The trend is similar when the spectral filtering bandwidth gets narrower. Hence, we demonstrate that the spectral filtering effect induced by the CFBG causes multi-pulsing. It is possible to further increase the single pulse energy by avoiding the strong spectral filtering effect.

2. Experimental setup and results

Figure 1 shows the experimental setup of a linear cavity configuration with polarization maintaining (PM) fibers. A

piece of 60-cm long highly Yb-doped PM fiber (250 dB/m at 975 nm) is pumped by a 976-nm single-mode laser diode. A half-wave plate (HWP) in combination with a polarization beam splitter (PBS) is used to ensure the excitation along the slow axis of the PM fiber. The single-mode fibers (SMFs) used are PM980 fibers with a mode field diameter of 6.6 μm at 980 nm. A SESAM (Batop GMBH, SAM-1040-56-700fs) with a 34% modulation depth and a 70 $\mu\text{J}/\text{cm}^2$ saturation fluence is utilized for self-starting mode-locking. A PM-CFBG with -0.1-ps^2 dispersion is employed for dispersion compensation. When the NCD is zero, the effective cavity length is 3.7 m, corresponding to a repetition rate of about 40.6 MHz. The CFBG also acts as a Gaussian spectral filter with a 17-nm bandwidth and a 13% peak reflectivity centered at 1030 nm. To compensate for third-order dispersion, a hybrid grating-prism compressor with 1200 lines/mm gratings and SF11 prisms is used to compress the output pulses.

The NCD of this fiber laser can be tuned from -0.03 ps^2 to $+0.025\text{ ps}^2$ by altering the length of the SMF between the collimator and the YDF. For each NCD, the pump power threshold for mode-locking is slightly different owing to the splice loss and other intra-cavity loss. To obtain stable mode-locking throughout the dispersion regime, the pump power is increased from 80 mW. Figure 2 shows an overview of the 10-dB spectral width and dechirped 3-dB pulse duration of the output pulses versus the NCD at different pump powers. At 80-mW pump power, the laser operates in the single-pulsing state with large normal and anomalous dispersion. As the NCD decreases, the spectral width gradually increases, which is typical of a DM fiber laser^[24]. However, a further decrease in the NCD leads to the generation of multiple pulses. The double-pulsing state is observed with the NCD ranging from $-5.67 \times 10^{-3}\text{ ps}^2$ to $+6.48 \times 10^{-3}\text{ ps}^2$ (Figure 2(a), gray area). Figure 3(a) shows the spectrum and the autocorrelation trace of soliton molecules for $\beta_{\text{net}} = +7.52 \times 10^{-4}\text{ ps}^2$. The spectral modulation period is 0.74 nm, corresponding to a pulse separation of 4.8 ps. We also measure the output spectra for two critical

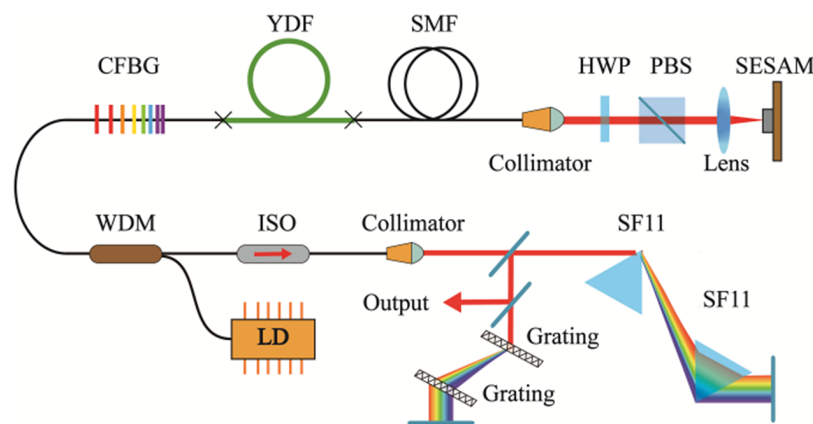


Figure 1. Experimental setup of the passively mode-locked all-PM fiber laser. LD, laser diode; WDM, wavelength division multiplexer; CFBG, chirped fiber Bragg grating; YDF, Yb-doped fiber; SMF, single-mode fiber; SESAM, semiconductor saturable absorber mirror; HWP, half-wave plate; PBS, polarization beam splitter; ISO, isolator.

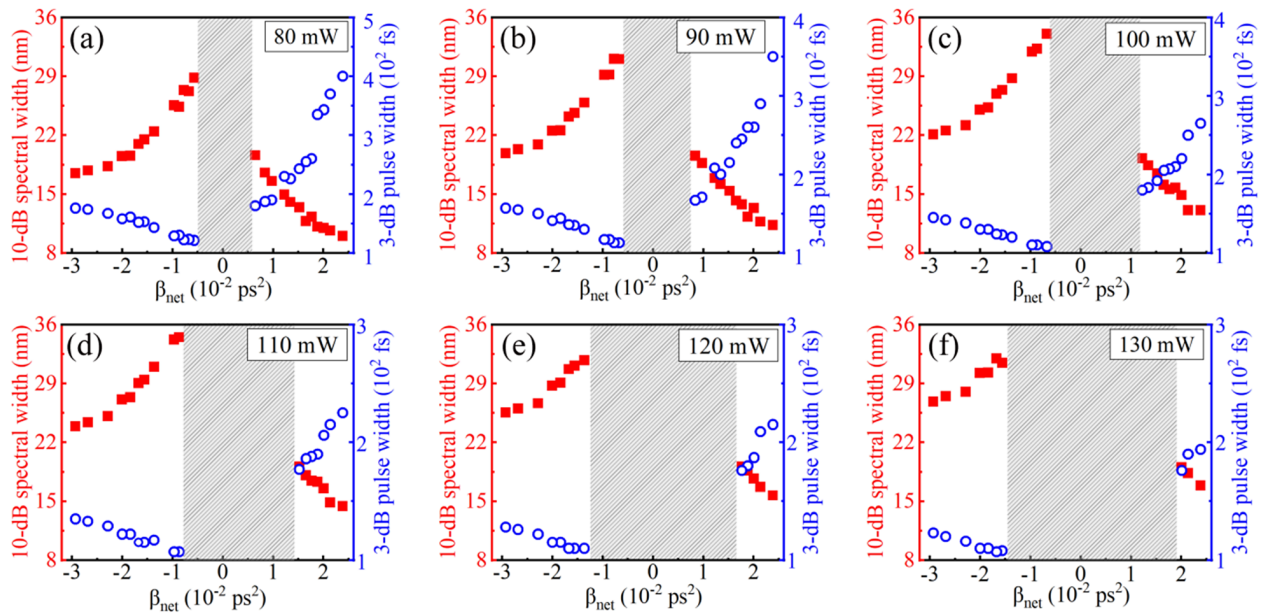


Figure 2. Spectral width at 10 dB (red solid squares) and dechirped pulse width at 3 dB (blue open circles) of the output pulses versus the NCD at a pump power of (a) 80 mW, (b) 90 mW, (c) 100 mW, (d) 110 mW, (e) 120 mW, and (f) 130 mW (gray area: multi-pulsing region).

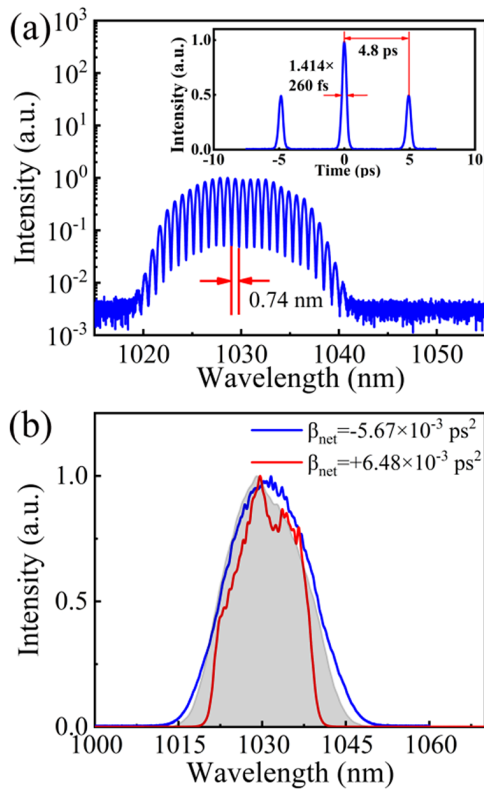


Figure 3. (a) Spectrum and autocorrelation trace of soliton molecules at 80 mW pump power. (b) Spectra of single soliton states for two critical NCD values at 80 mW pump power (gray area: CFBG reflection spectrum).

NCD values, as shown in Figure 3(b). For comparison, the measured CFBG reflection spectrum is also shown as the gray area. For $\beta_{\text{net}} = -5.67 \times 10^{-3} \text{ ps}^2$, the spectrum shows a Gaussian-like profile and fits well with the CFBG

reflection spectrum. However, for $\beta_{\text{net}} = +6.48 \times 10^{-3} \text{ ps}^2$, the spectral edges fit with a parabolic-like profile. Furthermore, the output spectrum is restricted by the strong filtering effect compared with the typical self-similar spectrum with a parabolic top^[26].

With the pump power rising, the multi-pulsing region is enlarged, as shown in Figure 2. Thus, the DM fiber laser shows different pump power thresholds for the double-pulsing state with different NCD values. With close-to-zero NCD, the critical pump power of the double-pulsing state is slightly larger than the mode-locking threshold. With a larger NCD, the stable area for the single-pulsing regime extends towards a higher pump power. For $\beta_{\text{net}} \leq -1.56 \times 10^{-2} \text{ ps}^2$ and $\beta_{\text{net}} \geq +2 \times 10^{-2} \text{ ps}^2$, the laser can operate in the single-pulsing state at a maximum pump power of 130 mW. Note that, the CSW at the critical point is around 30 nm in the anomalous dispersion regime and 19 nm in the normal dispersion regime, regardless of the pump power. We attribute multi-pulsing generation to the spectral filtering effect. When the spectral width gets broader, the strong dissipative effect of the filter induces more loss. Once the pulse breaks up into two pulses, the energy of each pulse is reduced, resulting in wider pulse duration and narrower spectral width. Thus, the pulses can experience reduced loss induced by the spectral filtering effect. When the pump power exceeds 130 mW, the single-pulsing state cannot be obtained throughout the entire dispersion range due to excess nonlinear phase accumulation from SPM^[27].

The spectral width becomes broader either as the NCD approaches zero or as the pulse energy increases. However, the spectral filter inside the cavity limits the maximum spectral width and the shortest pulse duration

Table 1. Overview of key parameters of mode-locked YDF lasers using a CFBG for dispersion management.

Net dispersion	Spectral width	Pulse width	Pulse energy	Average power	Reference
0.016 ps ²	12.3 nm	213 fs	160 pJ	4 mW	[22]
0.02 ps ²	10.4 nm	162 fs	27 pJ	0.5 mW	[28]
-1.96 ps ²	0.7 nm	2.7 ps	130 pJ	2.5 mW	[29]
-1.7 ps ²	0.65 nm	3.6 ps	22 pJ	1 mW	[30]
-0.004 ps ²	17 nm	139 fs	140 pJ	6 mW	[13]
-0.0167 ps ²	19.4 nm	108 fs	420 pJ	21 mW	This work

that can be achieved. At 80 mW pump power, the maximum FWHM spectral width of 17.7 nm is obtained for $\beta_{\text{net}} = -5.67 \times 10^{-3} \text{ ps}^2$. The pulses are dechirped to 124 fs with the hybrid grating-prism compressor, as shown in Figure 4(a). At 100 mW pump power, the widest spectrum of 20.6 nm is obtained for $\beta_{\text{net}} = -6.71 \times 10^{-3} \text{ ps}^2$. The pulses can be compressed to 108 fs, as shown in Figure 4(b). When the pump power increases to 130 mW, the maximum spectral width is 19.4 nm with $\beta_{\text{net}} = -1.67 \times 10^{-2} \text{ ps}^2$. The output pulses can be compressed to 108 fs, as shown in Figure 4(c). The autocorrelation trace fits well with a Gaussian function, indicating high temporal quality. The laser produces 21 mW average power, corresponding to a 0.42 nJ pulse energy. An overview of the key parameters of the mode-locked YDF lasers using a CFBG for dispersion management is given in Table 1.

3. Numerical simulation and results

We consider a linear DM laser, as shown in Figure 5(a), with a piece of YDF, a piece of SMF, a SESAM, and a CFBG. The CFBG model is split into a short dispersion compensating fiber (DCF), a Gaussian bandpass filter, and an optical coupler (OC). Each fiber segment is modeled via the modified nonlinear Schrödinger equation^[31]:

$$\frac{\partial A}{\partial z} + \frac{i}{2} \left(\beta^{(2)} + ig \frac{1}{\Omega_g^2} \right) \frac{\partial^2 A}{\partial \tau^2} = \frac{g}{2} A + \frac{\beta^{(3)}}{6} \frac{\partial^3 A}{\partial \tau^3} + i\gamma |A|^2 A, \quad (1)$$

where $A = A(z, \tau)$ is the field envelope with z as the propagation coordinate and τ as the time-delay parameter, $\beta^{(2)}$ and $\beta^{(3)}$ are the group velocity dispersion (GVD) and third-order dispersion, respectively, γ is the nonlinear parameter, and Ω_g is the gain bandwidth. The gain g is modeled by $g = g_0/(1+E/E_{\text{sat}})$, where g_0 is the small-signal gain, E is the intracavity energy, and E_{sat} is the saturation energy^[32]. Here E is calculated by $E = \iint |A|^2 d\tau + E_{\text{oppo}}$, where E_{oppo} is the energy of the pulses coming from the opposite direction of the gain fiber. The inclusion of E_{oppo} is necessary when the pulses experience significantly different losses on the two sides of the gain fiber. The reflection of the SESAM is modeled by $R = 1 - \Delta T/(1 + P_{\text{ave}}/P_{\text{sat}}) - \alpha_{\text{ns}}$, where ΔT is the modulation depth, P_{ave} is the average power, P_{sat} is the

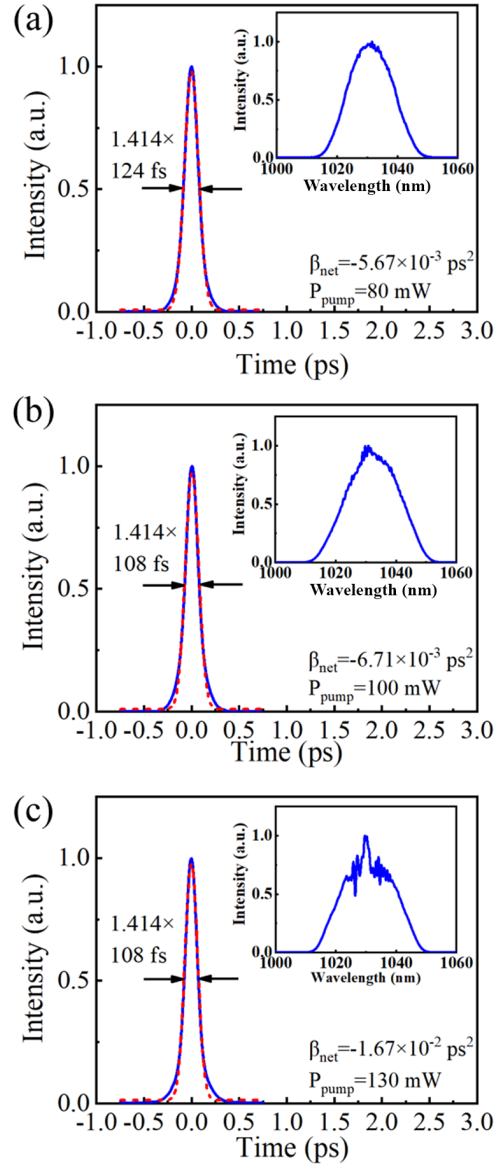


Figure 4. Autocorrelation traces of dechirped output pulses (blue solid lines) and Gaussian fitting curves (red dashed lines) at a pump power of (a) 80 mW, (b) 100 mW, and (c) 130 mW. Insets: corresponding spectra of output pulses.

saturation power, and α_{ns} is the nonsaturable loss. In the simulations, the parametric values of the YDF are $L_{\text{YDF}} = 0.6 \text{ m}$, $\Omega_g = 40 \text{ nm}$, $g_0 = 30 \text{ dB}$, and $E_{\text{sat}} = 0.2 \text{ nJ}$. For the SESAM, we set $\Delta T = 0.34$, $\alpha_{\text{ns}} = 0.22$, and $P_{\text{sat}} = 40 \text{ W}$, consistent with the experimental values. We consider an OC with a 90%

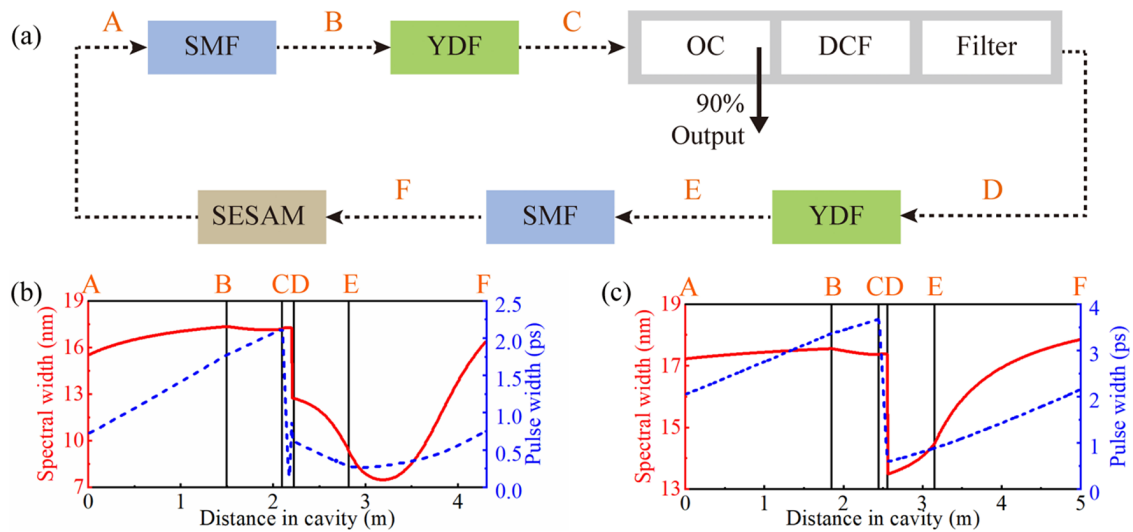


Figure 5. (a) Schematic of the numerical simulation model. Evolution of spectral width (red solid line) and temporal width (blue dotted line) when the NCD is for (b) $\beta_{\text{net}} = -1.1 \times 10^{-3} \text{ ps}^2$ and (c) $\beta_{\text{net}} = +1.5 \times 10^{-2} \text{ ps}^2$. YDF, Yb-doped fiber; SMF, single-mode fiber; SESAM, semiconductor saturable absorber mirror; DCF, dispersion compensating fiber; OC, optical coupler.

coupling ratio. For the DCF, we assume $L_{\text{DCF}} = 0.1 \text{ m}$ with a GVD of $-1 \text{ ps}^2/\text{m}$. The spectral filter has a 17-nm (FWHM) Gaussian profile centered at 1030 nm. Before the SESAM (point F), an intracavity loss of 2.2 dB is applied to model the loss induced by the coupling process and the polarizer. In the simulations, we use 2^{11} points, a 40-ps time span, and a 1-mm spatial step. The initial condition is a Gaussian pulse (10 ps, FWHM), injected at point D. The solution is assumed to be converged if the relative change of the pulse energy is lower than 10^{-9} .

Figures 5(b) and 5(c) show the intra-cavity evolution of stable single pulses with $\beta_{\text{net}} = -1.1 \times 10^{-3} \text{ ps}^2$ and $\beta_{\text{net}} = +1.5 \times 10^{-2} \text{ ps}^2$, respectively. The CFBG shows an obvious dissipative effect, and the pulse width reaches the minimum in the CFBG. For an anomalous NCD, the pulses are negatively chirped after the CFBG, and thus the pulses and the spectrum are compressed in the latter fiber segments (YDF and SMF). Subsequently, the spectrum experiences nonlinear broadening through the SPM when the chirp becomes positive. For a normal NCD, the pulses are positively chirped along the cavity, and hence the SPM leads to spectral broadening after the CFBG (Figure 5(c)).

To study the multi-pulsing dynamics in the DM fiber laser, we vary the NCD and the saturation energy E_{sat} to obtain different operation states. In Figure 6(a), white areas represent the stable multi-pulsing region. Near zero NCD, the laser generates multiple pulses with an extremely small E_{sat} . With a stronger NCD, the threshold for multi-pulsing operation shifts towards a higher E_{sat} , resulting in maximum spectral broadening through SPM. Therefore, pulses with the broadest spectrum are generated at the critical NCD. We observe that when E_{sat} is larger than 0.25 nJ, single pulses cannot be obtained throughout the NCD regime.

Thus, we set the maximum E_{sat} at 0.25 nJ and, hence, the maximum spectral width of 19 nm is obtained for both $\beta_{\text{net}} = -1.1 \times 10^{-3} \text{ ps}^2$ and $\beta_{\text{net}} = +1.5 \times 10^{-2} \text{ ps}^2$. To achieve a low timing jitter, it is preferable to operate the DM laser with an anomalous NCD. For comparison, we fix the NCD at $-1.1 \times 10^{-3} \text{ ps}^2$ and vary the spectral filter bandwidth and the saturation energy E_{sat} . Figure 6(b) shows the spectral width of the pulses at point D in the cavity. With a narrow filter, the multi-pulsing state operates at a low E_{sat} . A broadband spectral filter can support stable single pulses under a high E_{sat} . This trend is similar to the results observed by varying the NCD in Figure 6(a). To further investigate the filtering effect on multi-pulsing, numerical simulation is carried out at the critical E_{sat} for different filter bandwidths in the range of 1–40 nm. The spectral filtering exhibits different impacts depending on the filter bandwidth, as shown in Figure 6(c). For a filter bandwidth narrower than 9 nm, the laser operates in the multi-pulsing state when E_{sat} is at the mode-locking threshold. The strongly dissipative action of the filtering induces extra loss, leading to a decreased multi-pulsing threshold. For a filter bandwidth in the 9–40 nm range, the spectral width of the pulses at point D gets wider with an increased filter bandwidth. The dissipative filtering effect is still present, and it restricts the spectral broadening through SPM. Both the spectral width of the output pulses and the corresponding E_{sat} increase monotonically as the filter bandwidth gets wider. The spectral filtering results in multi-pulsing when the spectral width gets comparable with the filter bandwidth. The dissipative effect has a strong impact on the pulse-shaping mechanism, unlike in traditional DM fiber lasers where the pulses are only stabilized by a balance between GVD and SPM. Thus, the addition of the dissipative mechanism to DM cavities induces the generation

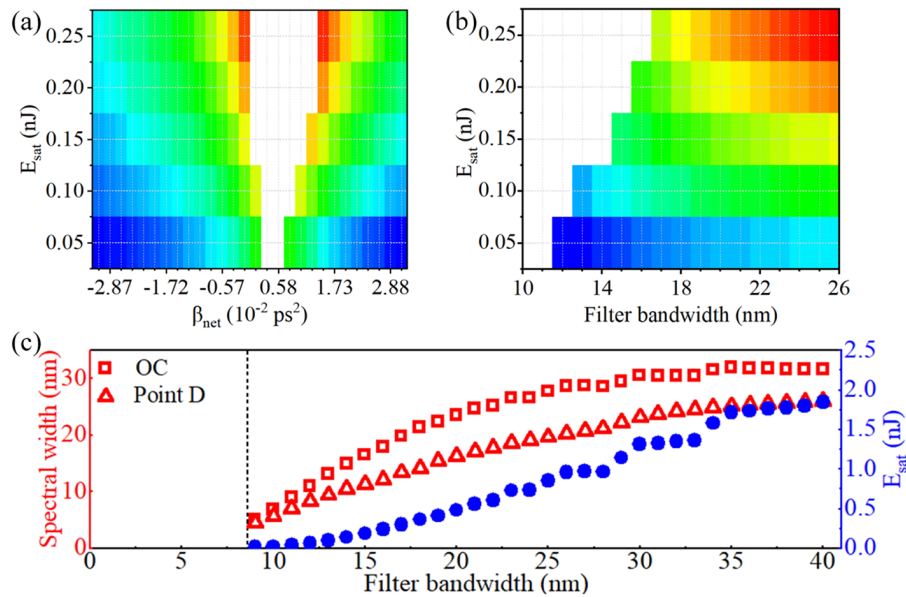


Figure 6. (a) FWHM spectral width of output pulses as a function of NCD and E_{sat} . Linear scale: 4 nm (white area: multi-pulsing region). (b) FWHM spectral width of pulses at point D as a function of filter bandwidth and E_{sat} . Linear scale: 8 nm (white area: multi-pulsing region). (c) FWHM spectral width of pulses at the OC (red open squares) and at point D (red open-triangles) at critical pump power and corresponding E_{sat} (blue solid circles).

of generalized dissipative solitons^[33]. The optimum condition where the shortest compressed pulses are obtained shifts from zero NCD to an anomalous NCD.

4. Conclusion

In this work, we experimentally demonstrate that the CFBG-induced spectral filtering effect can cause multi-pulsing in a DM mode-locked YDF laser. With an increased pump power, the spectral width keeps increasing until it reaches a critical point. And this CSW value is limited by the CFBG reflection bandwidth. By simulating this DM soliton laser with a split CFBG model, we demonstrate that the spectral filtering effect plays a decisive role in the multi-pulsing dynamics. The CSW at the critical point and the corresponding pump power are dependent on the spectral filtering bandwidth. Thus, CFBGs with broader reflection spectra can enable shorter compressed pulses and higher single-pulse energy. A recent work reports the management of the multi-pulsing state by using a fiber-based spectral filter in an all-normal dispersion fiber laser^[34], where the spectral filter plays an important role in stabilizing the pulses. Although a filter is not necessary for the DM soliton dynamics, the filtering effect still has a strong impact on the multi-pulsing process and hence a spectral filter with a tunable bandwidth can potentially control the multi-pulsing state.

Acknowledgements

This work was partially supported by the National Natural Science Foundation of China (NSFC) (Nos. U1730115,

61805174, and 61827821), the Tianjin Natural Science Foundation (No. 20JCQNJC01180), the Tianjin Research Program of Application Foundation and Advanced Technology of China (No. 17JCJQC43500), and the Research and Development Program in Key Areas of Guangdong Province, China (No. 2020B090922004).

References

1. N. R. Newbury and W. C. Swann, *J. Opt. Soc. Am. B* **24**, 1756 (2007).
2. S. A. Diddams, *J. Opt. Soc. Am. B* **27**, B51 (2010).
3. S. Kawawashi, *IEEE J. Quantum Electron.* **34**, 20640 (1998).
4. H. Bergeron, L. C. Sinclair, W. Swann, C. Nelson, J. Deschênes, E. Baumann, F. Giorgetta, I. Coddington, and N. Newbury, *Optica* **3**, 441 (2016).
5. X. Xie, R. Bouchand, D. Nicolodi, M. Giunta, W. Hänsel, M. Lezius, A. Joshi, S. Datta, C. Alexandre, M. Lours, P. Tremblin, G. Santarelli, R. Holzwarth, and Y. L. Coq, *Nat. Photon.* **11**, 44 (2016).
6. O. G. Okhotnikov, *Fiber Lasers* (Wiley, New York, 2012).
7. M. E. Fermann and I. Hartl, *IEEE J. Sel. Top. Quantum Electron.* **15**, 191 (2009).
8. K. Tamura, E. Ippen, H. Haus, and L. E. Nelson, *Opt. Lett.* **18**, 1080 (1993).
9. C. Nielsen, B. Ortaç, T. Schreiber, J. Limpert, R. Hohmuth, W. Richter, and A. Tünnermann, *Opt. Express* **13**, 9346 (2005).
10. P. Grellu and N. Akhmediev, *Nat. Photon.* **6**, 84 (2012).
11. Y. Song, C. Kim, K. Jung, H. Kim, and J. Kim, *Opt. Express* **19**, 14518 (2011).
12. L. Nugent-Glandorf, T. A. Johnson, Y. Kobayashi, and S. Diddams, *Opt. Lett.* **36**, 1578 (2011).
13. D. Yan, B. Liu, J. Guo, M. Zhang, Y. Chu, Y. Song, and M. Hu, *Opt. Express* **28**, 29766 (2020).
14. J. Kim and Y. Song, *Adv. Opt. Photon.* **8**, 465 (2016).
15. F. X. Kurtner, J. Der Au, and U. Keller, *IEEE J. Sel. Top. Quantum Electron.* **4**, 159 (1998).

16. J. M. Soto-Crespo, M. Grapinet, P. Grelu, and N. Akhmediev, *Phys. Rev. E* **70**, 066612 (2004).
17. D. Tang, L. M. Zhao, B. Zhao, and A. Q. Liu, *Phys. Rev. A* **72**, 043816 (2005).
18. F. Li, P. K. A. Wai, and J. N. Kutz, *J. Opt. Soc. Am. B* **27**, 2068 (2010).
19. W. H. Renninger, A. Chong, and F. W. Wise, *J. Opt. Soc. Am. B* **27**, 1978 (2010).
20. M. Alsaleh, T. Uthayakumar, E. T. Felenou, P. T. Dinda, P. Grelu, and K. Porsezian, *J. Opt. Soc. Am. B* **35**, 276 (2018).
21. K. Hill, F. Bilodeau, B. Malo, T. Kitagawa, S. Thériault, D. C. Johnson, J. Albert, and K. Takiguchi, *Opt. Lett.* **19**, 1314 (1994).
22. B. Ortaç, M. Plötner, T. Schreiber, J. Limpert, and A. Tünnermann, *Opt. Express* **15**, 15595 (2007).
23. K. Ennser, N. Zervas, and R. Laming, *IEEE J. Quantum Electron.* **34**, 770 (1998).
24. M. Baumgartl, B. Ortaç, J. Limpert, and A. Tünnermann, *Appl. Phys. B* **107**, 263 (2012).
25. J. Jeon, J. Lee, and J. H. Lee, *J. Opt. Soc. Am. B* **32**, 31 (2015).
26. F. Ilday, J. Buckley, W. Clark, and F. Wise, *Phys. Rev. Lett.* **92**, 213902 (2004).
27. H. Haus, K. Tamura, L. Nelson, and E. Ippen, *IEEE J. Quantum Electron.* **31**, 591 (1995).
28. H. Chang, Z. Cheng, R. Sun, Z. Peng, M. Yu, Y. You, M. Wang, and P. Wang, *Opt. Express* **27**, 34103 (2019).
29. L. Zhang, A. El-Damak, Y. Feng, and X. Gu, *Opt. Express* **21**, 12014 (2013).
30. O. Katz, Y. Sintov, Y. Nafcha, and Y. Glick, *Opt. Commun.* **269**, 156 (2007).
31. G. P. Agrawal, *Nonlinear Fiber Optics* (Academic Press, San Diego, 2009).
32. I. A. Yarutkina, O. V. Shtyrina, M. P. Fedoruk, and S. K. Turitsyn, *Opt. Express* **21**, 12942 (2013).
33. W. H. Renninger, A. Chong, and F. W. Wise, *IEEE J. Sel. Top. Quantum Electron.* **18**, 389 (2012).
34. A. Khanolkar and A. Chong, *Opt. Lett.* **45**, 6374 (2020).